Turbulent Mixing at the Pacific Subtropical Front

ROLF G. LUECK

Chesapeake Bay Institute, The Johns Hopkins University, Baltimore, Maryland

(Manuscript received 27 July 1987, in final form 8 February 1988)

ABSTRACT

Some advection of water across the North Pacific subtropical front occurs by the subduction of surface mixed layers from the north side of the front underneath surface waters on the south side. Cross-frontal advection in the thermocline is obscure because waters from both sides of the front follow a single trajectory in θ–S space. When winds are less than 10 m s^{-1}, turbulence between these layers is too small to generate significant vertical diffusion. However, typical winter storms could mix these layers, in less than 20 days, to form a single homogeneous surface layer up to 145 m thick. When surface winds are too weak to maintain mixing over the entire depth of a surface mixed layer, turbulence associated with internal waves in the top of the thermocline contributes to the restratification of the surface layers. On a sampling grid of 37 km, there is no evidence for a systematic geographic variation of the rate of dissipation of kinetic energy. The rate of dissipation near the front is larger than in low energetic regions like the Sargasso Sea or off Vancouver Island, but smaller than in highly energetic ones such as the Equatorial Undercurrent or warm-core rings.

1. Introduction

One of the notable surface features of the North Pacific is the subtropical front separating warm ($T > 18$°C) and saline ($S > 34.8$) North Pacific Central Water in the south from cooler ($T < 18$°C) and fresher ($S < 33.8$) water to the north. Meridional variations of surface heating and evaporation produce horizontal gradients of surface temperature and salinity which are not density compensated. These gradients are concentrated by the convergence and deformation of the large scale flow field (Roden 1980a). The convergence is primarily produced by meridional gradients in the Ekman flow induced by north–south gradients of the surface stress. From a basin perspective, the front tends to be zonal along 31°N.

In the winter of 1980 a major observational program, called FRONTS 80, was started to study the structure and evolution of the subtropical front near 154°W. Using a 37 km sampling grid, Roden (1981) observed in January of 1980 maximum horizontal differences of 1.7°C, 0.6 psu (practical salinity units) and 0.4 kg m^{-3} for temperature, salinity and sigma-t, respectively. The front was not a simple zonal feature. It had a meander of wavelength 180 km and amplitude of 55 km centered around 30°N. The largest horizontal gradients were found below the surface mixed layer. Gradients of up to 0.39°C km^{-1} across highly contorted filaments are evident in sea surface temperature data measured by satellite (van Woert 1982).

Large scale convergence in the direction of ambient property gradients tends to intensify these gradients into a front. The shearing and straining of the frontal property gradients by eddies and meanders of the flow field near a front increases further the wavenumber and the magnitude of these gradients. Irreversible mixing by three dimensional turbulence may then transform these waters into a type with intermediate properties. Increased levels of turbulence, relative to less energetic environments, are therefore expected near a front and frontogenesis may, in part, be balanced by turbulent diffusion. In January and February of 1980, 37 profiles of microstructure velocity and temperature were made in the North Pacific Subtropical front, in conjunction with CTD measurements (Roden 1981). The microstructure data are used here to 1) present evidence for the subduction of surface mixed layers across the front, 2) estimate the rate of vertical diffusion of these subducted layers, 3) show evidence of mixing forced by near-inertial waves, 4) show an absence of systematic cross-frontal variations in the rate of dissipation of kinetic energy, and 5) make a comparison of dissipation rates against other oceanic regions.

2. Instrumentation

The microstructure data were collected with the free-fall vehicle *Camel II*. Typical use of this instrument and data processing are described by Lueck et al. (1983). While it descended at a speed of 0.65 m s^{-1}, *Camel II* sensed two components of horizontal velocity using air-foil probes (Osborn and Crawford 1980), temperature using an FP-07 thermistor, pressure using a strain gauge transducer and accelerations orthogonal

Corresponding author address: Dr. Rolf G. Lueck, Chesapeake Bay Institute, The John Hospkins University, Baltimore, MD 21211.

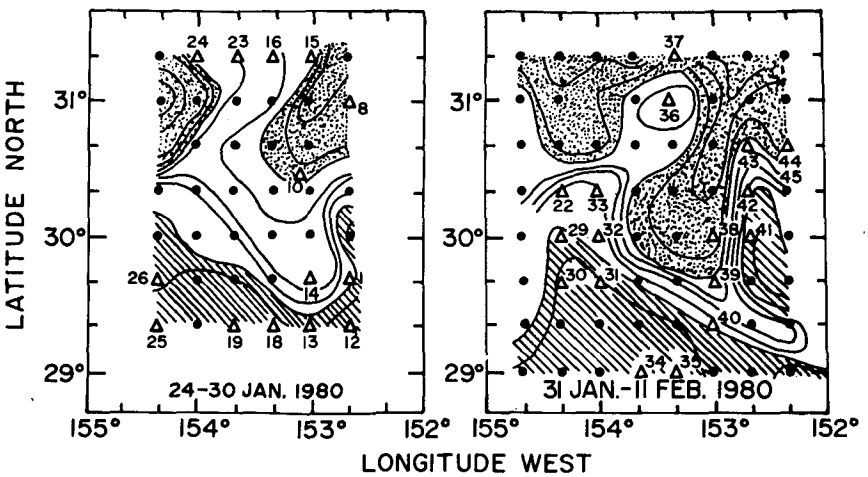

FIG. 1. Sea surface salinity in the study area. Solid circles represent CTD stations (Roden 1981); open triangles show the locations of *Camel II* profiles made at all Camel stations. Phase I was terminated on 30 January because of storms with winds exceeding 30 m s^{-1}. Phase II (31 January to 11 February) shows frontogenesis by the southward advection of surface waters from north of the front. Salinity contours south of the 35 surface isohaline show little difference between the two survey phases. Hatched regions mark salinity greater than 35.1; stippled ones less than 34.9; the contour interval is 0.05.

to its axis using two accelerometers. The spatial resolution of the shear probes is 75 cpm (Ninnis 1983). Through a system of in situ analog processing, FM telemetry, and analog to digital conversion, the data were logged as 12 bit words on 9-track tapes in real time. Temporal derivatives have been converted into spatial ones assuming a "frozen" field. The data were sampled 400 times per second which was equivalent to approximately one point every 0.0016 m.

The rate of dissipation of turbulent kinetic energy, ϵ, in units of watts per cubic meter, is estimated using the isotropic formula

$$\epsilon = (15\rho\nu/4)[\langle(\partial u/\partial z)^2\rangle + \langle(\partial v/\partial z)^2\rangle] \quad (1)$$

where ν is the kinematic viscosity corrected for its temperature dependence, $\rho = 1025$ kg m^{-3} is the density of water and the angled braces, $\langle\ \rangle$, denote a spacial average. The smallest dissipation rates, 2×10^{-7} W m^{-3}, represent the noise level of the instrumentation which is caused by wobble and other spurious motions of the vehicle (Moum and Lueck 1985). The noise reported by Lueck et al. (1983) for the same instrumentation is smaller by a factor of 2 because a high pass digital filter designed to remove signals induced by the wobble of the instrument was not used on the dataset reported here.

3. Data

The data were collected in two phases at the locations shown in Fig. 1. During the first phase, lasting for 7 days and spanning drops 8 through 26, the front was weak and winds were moderate, reaching up to 16 m s^{-1} (Fig. 2). Two storms with westerly winds of up to 26 m s^{-1} followed the first phase. During the second phase, lasting 12 days and spanning drops 28 through 45, the surface signature of the front had intensified relative to the first phase and winds reached 26 m s^{-1}. The most severe winds caused temporal gaps in the sequence of profiles. The picture obtained is only quasi-synoptic. Turbulence profiling was only possible when winds were less than 15 m s^{-1}, and the most intense mixing events may have been missed. Between the two phases one profile was made during wind speeds of 15 m s^{-1}. The time, location, mixing layer depth and its

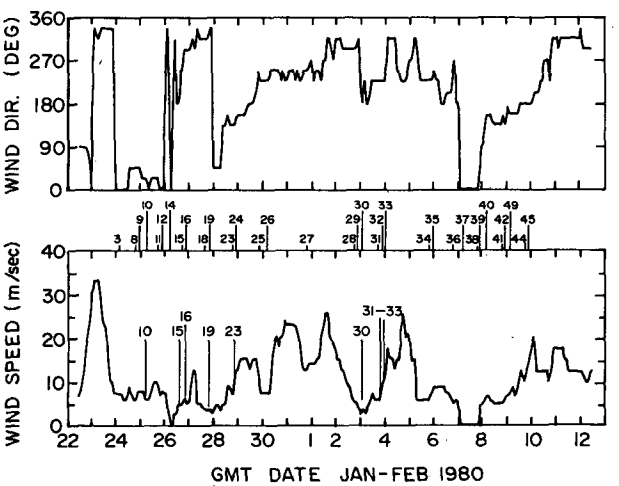

FIG. 2. Temporal location of Camel profiles and surface wind speed and direction (after Roden 1981).

average dissipation, wind speed and the distance of the profiles from the front are given in Table 1.

a. *Evidence for subduction*

Profiles near the front, here defined by the 35.0 isohaline after Roden (1981), frequently show a mixed layer between the surface mixed layer and the seasonal thermocline. The phrase "mixed layer" is used to identify quasi-isothermal layers or layers of low stratification. Turbulence and mixing are not implied. The microstructure from drop 18 (Fig. 3), made 35 km south of the front shows a nearly isothermal surface layer 30 m thick with a temperature of 18.70°C. A transition layer 25 meters thick separates the surface layer from a subsurface mixed layer with a temperature of 18.0°C. The subsurface layer spans from 55 to 155 m. The 0.7°C temperature difference between the surface and subsurface mixed layers cannot be explained by local vertical heating and must have resulted from the cross-frontal advection of surface waters. Velocity microstructure is present throughout this three-layer system and is most intense in the surface layer. Temperature gradient microstructure is significantly only above 100 m. Between 100 and 150 m the water is very well mixed and three-meter averages of temperature are 17.988 ± 0.003°. The presence of velocity microstructure and microscale temperature inversions (bipolar vertical temperature gradient) are evidence of a downward turbulent transport of heat through the transition layer. There is velocity microstructure from the surface to a depth of 172 m in the seasonal thermocline. The velocity microstructure decreases sharply 20 m below the bottom of the lower mixed layer where the water is 2° cooler than in that mixed layer. Therefore, there is a turbulent heat flux into the thermocline. The profile was made at 0815 LST under winds of 4 m s^{-1} (Table 1), so that wind forcing was negligible, but convective stirring forced by surface cooling may have been important (Moum and Caldwell 1986). There is some evidence for convective cooling in the temperature signal which increases by 0.020°C from the surface to 30

TABLE 1. Summary of *Camel II* profiles during FRONTS-80. The mixing layer depth is the depth at which the dissipation drops below 5×10^{-7} W m^{-3} or the temperature is 0.1°C less than at the surface. Wind speed after Hayes et al. (1981). The distance of the stations from the front is measured to the 35 psu surface isohaline; N and S indicate the origin of the surface water and not the geographic direction to the front.

Drop	CTD station	Longitude (deg-min W)	Latitude (deg-min N)	U_{10} (m s^{-1})	h_{ML} (m)	$10^5 \langle\epsilon\rangle_{ML}$ (W m^{-3})	Front (km)
3	4	130-16.0	33-04.8	2.5	75	1.1	∞
4	5	135-59.3	33-19.9	15	125	14.9	∞
7	9	152-38.4	32-39.9	8	35	57.3	∞
8	14	152-39.5	30-59.3	6	130	2.8	65 N
10	16	153-10.4	30-33.6	8	20	9.9	35 N
11	19	152-39.9	29-40.3	9	110	6.0	15 S
12	20	152-43.0	29-17.8	8	90	3.1	35 S
13	21	153-00.9	29-18.6	8	30	3.6	30 S
14	22	153-01.1	29-41.6	3	0		10 N
15	27	152-57.2	31-20.1	5	130	8.8	0
16	28	153-19.1	31-19.9	5	145	0.6	120 N
18	34	153-19.8	29-20.1	4	35	8.1	35S
23	41	153-38.0	31-18.5	8	150	7.9	100 N
24	42	153-58.0	31-21.0	13	110	17.8	100 N
25	49	154-21.7	29-18.6	9	50	6.4	100 S
26	50	154-21.1	29-38.9	7.5	30	11.5	75 S
27	56	154-38.8	28-58.7	14	125	10.4	60 S
28	67	154-13.8	30-14.4	7	151	9.7	10 S
29	68	154-21.6	29-59.9	5	115	1.5	35 S
30	69	154-20.4	29-39.9	3.5	20	1.6	55 S
31	74	153-59.6	29-41.9	7	45	25.4	30 S
32	75	154-02.1	30-00.9	7	70	11.4	10 S
33	76	153-58.3	30-20.1	11	80	18.3	20 S
34	87	153-40.1	29-00.2	6	60	13.9	75 S
35	88	153-19.7	29-00.6	7	75	4.0	65 S
36	94	153-24.1	31-05.1	6	40	0.9	60 N
38	100	153-00.0	29-59.4	0	35	0.5	20 N
39	101	152-59.5	29-40.0	3	30	2.0	20 N
40	102	153-00.7	29-19.8	6	20	4.6	20 S
41	107	152-41.3	30-01.4	5	35	8.2	20 S
42	108	152-41.1	30-20.3	6	20	1.4	10 S
43	109	152-39.0	30-39.7	8	35	4.4	10 N
44	114	152-18.0	30-40.7	13	35	1.8	20 N
45	114	152-15.3	30-40.4	15	55	0.2	20 N

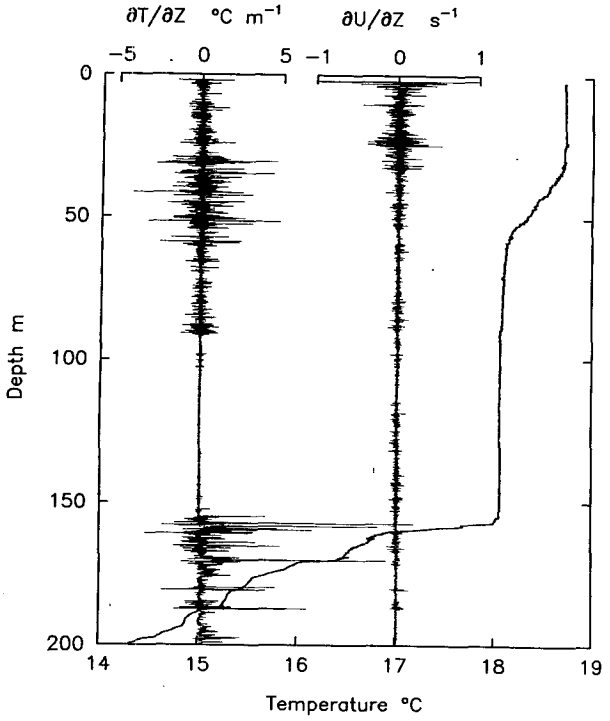

FIG. 3. Profile of the microstructure of shear, temperature and its gradient 35 km south of the front. Between 100 and 150 m, temperature gradients microstructure is near the noise level, indicating that the water is very well mixed.

m. The transition layer is a barrier to the downward flux of negative buoyancy forced by surface cooling (if any is present) and should tend to decouple the lower layer from direct and local atmospheric forcing. Turbulence in the transition and the lower layer must have been generated by shear from internal waves, the relative motion of subduction, or both.

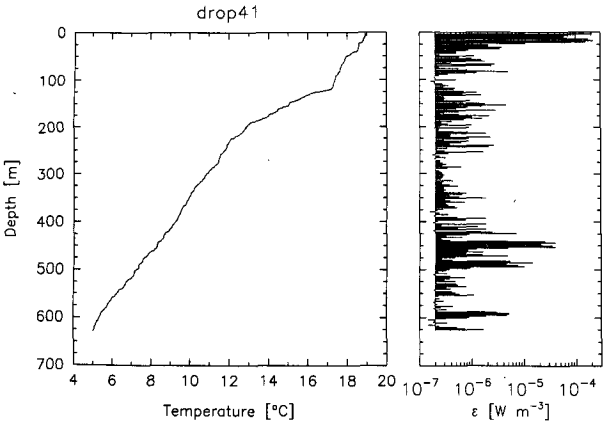

FIG. 5. As in Fig. 4, but in a region of very strong frontal gradients. There is considerable stratification even in the subsurface layer.

Near surface mixed layers, not in contact with the local surface, were observed in 12 of the 37 profiles made near the subtropical front. During the second phase, the surface layers are measurably stratified, but many of the subsurface layers are still nearly isothermal (drop 40, Fig. 4). In the region of strongest frontal gradients (30°N, 152°40′W, second phase) the front actually lies north–south and the surface and subsurface layers tend towards uniform stratification (drops 41 and 42, Figs. 5 and 6). The cross-frontal penetration of three subsurface mixed layers is evident in CTD data (Roden, personal communication 1983) on a zonal section along 29°20′N (Fig. 7), nominally parallel to the front. Layers are present at Camel drops 13, 18 and 19. The station spacing of 35 km is too large to allow a resolution of the width of the layers. A meridional section along 153°W (Fig. 8), nominally across the front, shows that the submerged mixed layer in drop 13 could outcrop between the location of drops

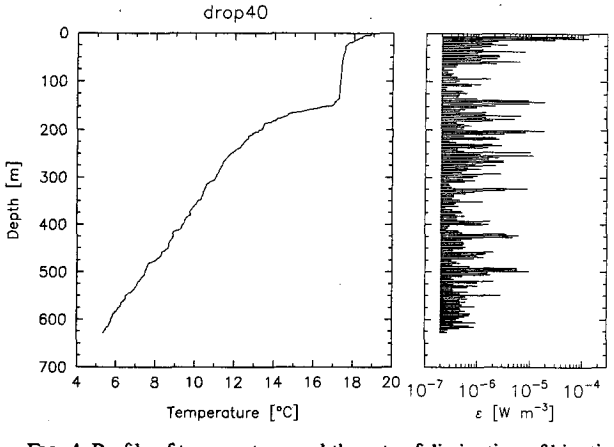

FIG. 4. Profile of temperature and the rate of dissipation of kinetic energy on the south side of the front during the second phase. The surface layers have stratified, but the subsurface layers are still quasi-isothermal.

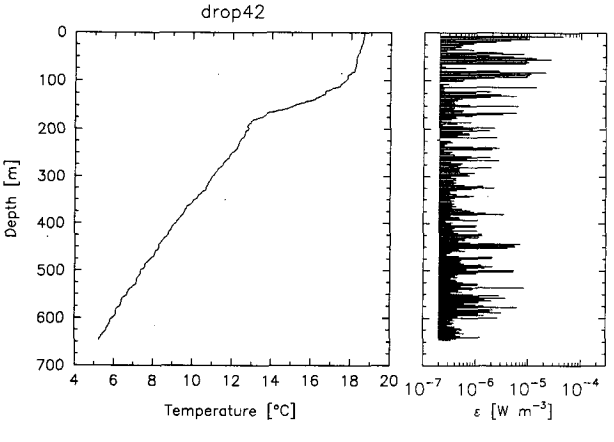

FIG. 6. As in Fig. 5, but at the 35 surface isohaline used to define the position of the front. There is considerable stratification in the near surface layers and there are patches of dissipation separate from the mixing layer contacting the surface.

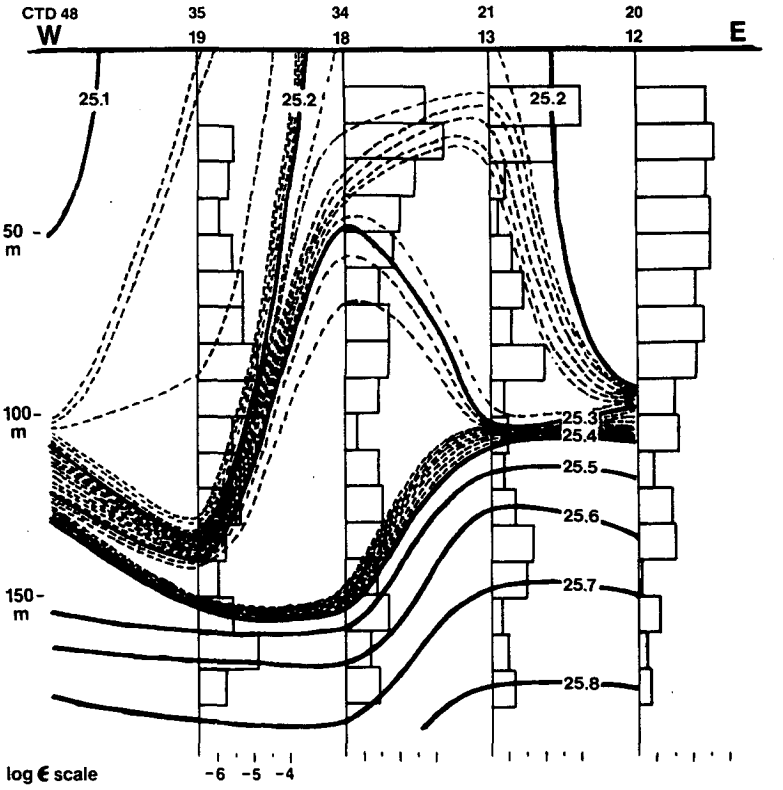

FIG. 7. Zonal section of potential density and 10 m averages of dissipation along 29°20'N, nominally parallel to the front. Subducted mixed layers are evident at Camel profiles 13, 18 and 19.

13 and 14 and thus may have its origin less than 35 km from its point of observation. By tow-yowing a CTD, Flament, Armi and Washburn (1985), were able to connect unambiguously subsurface filaments about 10 m thick to a surface convergence zone in the California current system. Given the extreme thickness of the layers at the subtropical front and their proximity to surface water of equal temperature, they must also be formed from surface mixed layers forced under the buoyant side of the front by surface convergence. No subducted layer was ever observed twice during the entire cruise. The horizontal limit of subduction must be less than 35 km and any attempt to study its detail requires a horizontal resolution much finer than the station spacing used in this study.

The subduction and the subsequent horizontal advection of surface mixed layers along a nearly isopycnal trajectory does not lead to significant vertical inversions of temperature or salinity. The θ–S characteristics of several cross-frontal hydrographic stations (Fig. 9) show little difference between stations spanning the front. The θ–S properties of water south of the front follows an almost linear trajectory to warmer and more saline values compared to water north of the front. This contrasts with cross-frontal intrusions across the Gulf Stream, for example, which lead to distinct water type anomalies. It is thus possible that thermocline water also penetrates across the front, but such intrusions are not readily apparent in the hydrographic area. It is the unique signature provided by the nearly isothermal structure of surface layers that permits us to identify the cross-frontal flow.

b. *Vertical turbulent diffusion*

The subduction of surface layers near the front converts relatively large horizontal property gradients into even larger vertical gradients which are susceptible to vertical diffusion and irreversible dissipation by small-scale turbulence. Is the observed turbulence intense enough to diffuse the vertical gradients produced by the subduction? The transition layers are almost always turbulent. The mean dissipation rates are 1.5×10^{-6} to 2.5×10^{-4} W m^{-3}, and are frequently comparable to values from the local surface layer (Table 2). An estimate of the time scale for the turbulent diffusion will be made with the data from drop 18 (Fig. 10) because it has the most clearly defined three-layer structure above the seasonal thermocline. Laboratory studies of stratified turbulent flow (Stillinger et al. 1983; Rohr et al. 1987) show that if the dissipation exceeds a value of $\epsilon_c = 16\rho\nu N^2$ then, the turbulence is suffi-

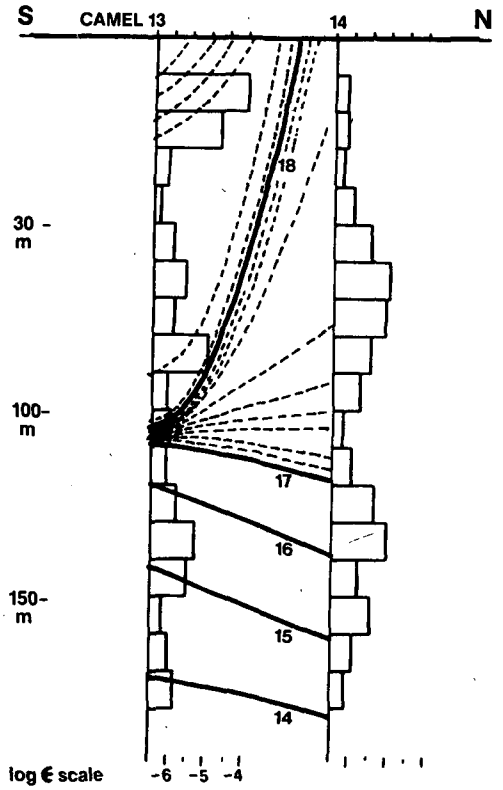

FIG. 8. Meridional section of potential temperature and 10 m averages of dissipation along 153°W. The subducted layer at Camel drop 13 must have its surface origin between drops 13 and 14, less than 35 km from its point of observation.

ciently intense to support a downward flux of buoyancy. In the transition layer, the buoyancy frequency is 6×10^{-3} s^{-1} (Roden 1980b), $\epsilon_c = 0.6 \times 10^{-6}$ W m^{-3} and the average dissipation is $20\epsilon_c$. Therefore, the

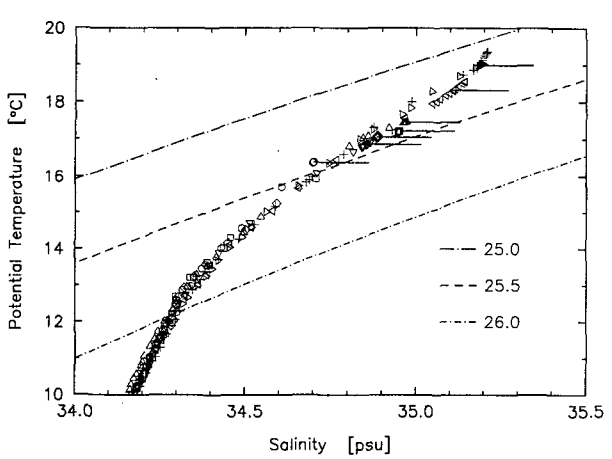

FIG. 9. Ten meter averages of potential temperature and salinity from eight stations along a meridional section at 154°20'W. Horizontal bars make the surface values and the three curves are isopycnals. Horizontal changes follow vertical changes closely and so, cross-frontal advection does not generate θ–S anomalies.

TABLE 2. Subducted surface layers. The vertical eddy diffusivity, K_ρ, is estimated from $0.2\langle\epsilon\rangle\,(\rho\,\langle N^2\rangle)^{-1}$ (Osborn 1980; Oakey 1985). Layer 1 is the surface "mixed" layer and absent on some profiles. Layers 2 and 3 are the transition and the submerged mixed layers, respectively. Profile 44 showed a second transition and submerged layer. A - = no data.

Drop	Layer	Δz (m)	$\langle\partial T/\partial z\rangle$ (°C m^{-1})	$10^7\langle\epsilon\rangle$ (W m^{-3})	$10^6\langle N^2\rangle$ (s^{-2})	$10^4 K_\rho$ (m^2 s^{-1})
13	1	15	0.0013	-	2	
	2	17	0.013	440	23	3.7
	3	60	0.002	17	0	
15	1	72	0.0001	830	0	
	2	35	0.01	1540	3	100
	3	9	0.002	8	0	
18	1	36	0.003	810	0	
	2	19	0.022	103	35	0.6
	3	95	0.001	30	0	
25	1	38	0.0006	760	2	
	2	10	0.009	400	30	2.6
	3	17	0.003	30	5	1.2
26	1	14	0.0008	1460	5	57
	2	19	0.011	970	22	8.6
	3	63	0.001	335	2	
34	1	30	0.001	1800	5	70
	2	5	0.020	2400	17	28
	3	16	0.001	1500	8	37
36	1	50	0.0007	70	1	
	2	9	0.030	15	18	0.2
	3	79	0.012	17	10	0.3
40	1	0	-	-	-	
	2	29	0.050	330	51	1.3
	3	106	0.0027	13	3	0.8
41	1	17	0.007	1200	2	
	2	8	0.034	1300	24	11
	3	14	0.007	24	5	0.9
42	1	0	-	-	-	
	2	51	0.008	35	13	0.5
	3	30	0.004	73	6	2.4
43	1	66	0.002	250	3	16
	2	21	0.027	450	24	3.7
	3	13	0.006	9	7	0.3
44	1	20	0.003	2000	11	35
	2	13	0.018	2500	30	16
	3	40	0.003	3	4	0.1
	4	10	0.027	20	18	0.2
	5	36	0.007	21	7	0.6

transition layer has a downward flux of heat and is considered "actively" turbulent. The upper limit of the vertical eddy diffusivity is $K_H = 0.2\epsilon\rho^{-1}N^{-2} = 0.6 \times 10^{-4}$ m^2 s^{-1} (Osborn 1980; Oakey 1985). The e-folding time for diffusing the surface and the subsurface layers into a single homogeneous layer is $\Delta H/Q = 150$ days, where ΔH is the total heat that must be transported vertically and Q is the vertical turbulent flux. The parameters used to estimate ΔH and Q are given in Table 3. The diffusive time scale of 150 days is much larger than the time of 10 days during which the front intensified between the first and second phase of the survey. Therefore, even though the transition layer is

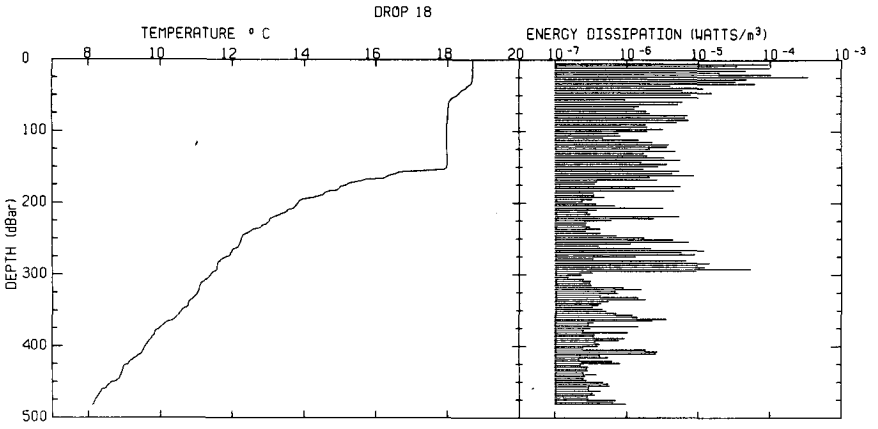

FIG. 10. Profile of temperature and the rate of dissipation of kinetic energy for drop 18 (Fig. 3). Dissipation is largest in the surface mixing layer, decreases in the transition layer and is still smaller in the lower quasi-isothermal layer. However, all dissipations are more than a decade above the noise level.

actively turbulent, the observed turbulence is not intense enough to make it a factor in frontogenesis.

An alternate mechanism for mixing the subducted and the surface layers is local atmospheric forcing. The work done on the ocean by the wind field is proportional to the wind speed cubed. Eleven meters per second is the highest wind speed for which a dissipation profile has been reported (Moum and Caldwell 1985). Drop 27 (Fig. 11) was made at the front during wind speeds of 15 m s^{-1}, about the highest speed at which a profile can be made with *Camel II*. Twenty-four hours earlier winds had reached 25 m s^{-1} (Fig. 2). We cannot be certain that this station had a subducted layer, mixing may have already obscured the evidence, but the temperature gradients above 120 m are comparable to the gradients in transition layers—see, for example, drop 18 (Fig. 10). The water column is intensely turbulent to a depth of 125 m. The upper 25 m is nearly isothermal and has a temperature of 19.54°C. Between 30 and 116 m temperature decreases, somewhat irregularly, from 19.52 to 18.66°C for a mean gradient of 0.010°C m^{-1}. The seasonal thermocline starts at 116 m and dissipation reaches a local maximum between 116 and 125 m. We will divide the water column into three layers: the upper 30 m, the gradient layer from 30 to 116 m and the top of the thermocline that is turbulent from 116 to 125 m. The Rohr et al. criterion, $\epsilon > \epsilon_c$, is satisfied well in the top two layers and satisfied by a factor of 4 in the thermocline layer. The *e*-folding time for mixing the upper 125 m into one homogeneous layer is 24 days (Table 4). More intense mixing might have occurred during the previous two days when winds reached 25 m s^{-1}. If turbulent diffusion was a little larger than at the time of drop 27, by a factor of 2, say, then air–sea interaction is a significant mechanism mixing the *horizontal* temperature (and other passive) anomalies at the front by *vertical* turbulent diffusion. Several turbulent and well mixed surface layers 145 m thick were observed (Fig. 12), indicating that the homogenization of the surface and subducted layers is possible, but evidently only by local atmospheric forcing.

Drop 27 (Fig. 11) is an example of vigorous mixing of near surface stratified waters forced by local air–sea interaction, but on the whole, dissipation rates in the surface layer at the front are not significantly different from previously reported values. There have been three attempts to relate the wind speed at 10 m to the integral

TABLE 3. Parameters used to estimate ΔH and Q. Dissipation, buoyancy frequency, eddy diffusivity $K_H = 0.2\epsilon\rho^{-1}N^{-2}$ and average temperatures T_i observed in surface and near surface layers from drop 18. Adiabatic mixing would produce a final temperature of 18.2°C and change the heat content as indicated. The *e*-folding time for adiabatic mixing is 150 days, given the turbulent flux at the time of observation and an infinite eddy diffusivity in the two well mixed layers.

Layer	ΔZ (m)	$10^7\epsilon$ (W m^{-3})	10^6N^2 (s^{-2})	10^4K_H (m^2 s^{-1})	T_i (°C)	T_f (°C)	ΔT (°C)	ΔH (10^6 J m^{-2})
Surface	36.5	810	0	∞	18.70	18.20	−0.50	−73
Transition	19.0	103	35	0.6	18.35	18.20	−0.15	−6
Subsurface	95.4	30	0	∞	17.99	18.20	0.21	79

Note: $\Delta H \approx 80 \times 10^6$ W s m^{-2}; $Q = \rho c K_H dT/dz = 6$ W m^{-2}; $\tau = \Delta H/Q \approx 150$ days.

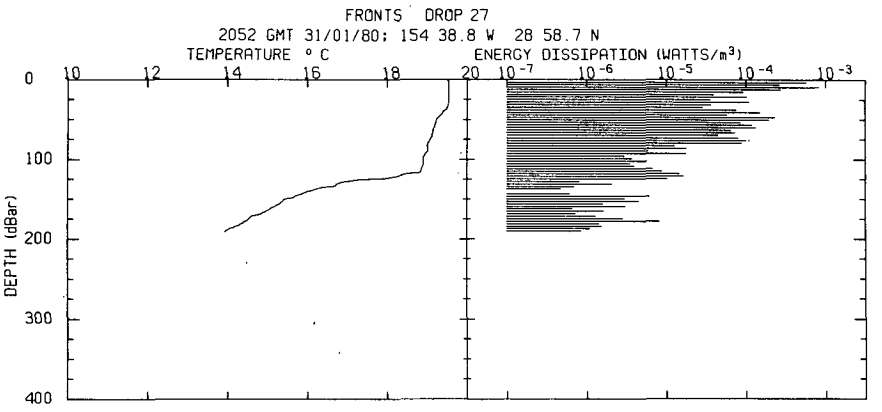

FIG. 11. Profile made during winds of 15 m s^{-1}, 24 hours after winds had peaked to 25 m s^{-1}. The water column is intensely turbulent to 125 m depth. The concurrence of stratification and vertically contiguous turbulence is evidence of vertical diffusion driven by air–sea interaction.

rate of dissipation in the surface mixing layers. The ratio, γ, of the depth integrated dissipation divided by the wind power, $\tau \cdot U_{10} = \rho_a C_D U_{10}^3$ was observed to be 0.92% between 10 and 110 m by Moum and Caldwell (1985), 1.6% between the surface and the base of the mixing layer by Oakey and Elliott (1982), and 0.6% between 15 and 90 m by Grant et al. (1968). Available energy produced by the surface buoyancy flux was not included in the ratio γ. There is clear evidence for increased dissipation rates at night compared to daylight hours (Moum and Caldwell 1985; Shay and Gregg 1986), but the daily averages of dissipation from Moum and Caldwell were proportional to wind speed cubed. The integral of dissipation over the surface mixing layers for all profiles is plotted (Fig. 13) against $U_{10} \cdot \tau$. To compute the integrals, the average observed dissipation in the mixing layers was multiplied by the depth of the layer. Ignoring the "flyers" in the lower right-hand corner of Fig. 13, the arithmentic mean of the ratio $h\langle\epsilon\rangle/U\tau$ is 1.4% and the geometric mean ratio is 0.8%.

c. *The role of near-inertial shear*

Not all nearly isothermal layers in contact with the atmosphere are turbulent. The temperature at the surface in drop 10 (Fig. 14) is 17.243°C, increases to 17.249°C at 11 m and then monotonically decreases to 17.100°C at 123 m depth. Above 120 m the buoyancy frequency varies between 0 and 2×10^{-3} s^{-1}. The rate of dissipation is large between the surface and 22 m where it has a mean of 1.1×10^{-4} W m^{-3}, it then decreases abruptly by a factor of 100 and is significant in the thermocline only between 130 and 136 m where the largest value for drop 10 is observed. The large decrease in dissipation at 22 m is noteworthy in that it can not be attributed to stratification, there being virtually none. The dissipation layer in the thermocline is at a temperature of 15.5°C, 1.7°C colder than the surface layer. Simultaneous measurements with expendable current profilers (Kunze, personal communication) show a strong near-inertial shear feature, approximately 20 m thick, in the top of the thermocline at about the same depth. The thermocline turbulence cannot be a result of air–sea interaction at the time of observation because the low level of turbulence in the bulk of the mixed layers means that there is no stress in the mixed layer below 20 m. The thermocline turbulence must therefore be generated by internal waves, very likely the near-inertial wave observed by Kunze and Sanford. Turbulence coincident with near-inertial shear has recently been reported by Gregg et al. (1985).

The profile obtained from drop 10 is not unique. Nine other drops revealed surface layers, many over 90 m thick, that are nearly isothermal, but have dissipation rates near the noise level below a shallow and turbulent surface layer. These layers were once well mixed, but have restratified since the source of energy

TABLE 4. Drop 27, as in Table 3 except, wind speeds were 15 m s^{-1}, down from 25 m s^{-1} 24 hours earlier.

Layer	ΔZ (m)	$10^7\epsilon$ (W m^{-3})	$10^6 N^2$ (s^{-2})	$10^4 K_H$ (m^2 s^{-1})	T_i (°C)	T_f (°C)	ΔT (°C)	ΔH (10^6 J m^{-2})
Surface	30	2560	0	∞	19.53	19.14	−0.39	−47
Transition	86	607	20	5.9	19.11	19.14	−0.03	10
Subsurface	9	136	130	0.2	18.14	19.14	1.00	36

Note: $\Delta H \approx 50 \times 10^6$ W s m^{-2}; $Q = \rho c K_H dT/dz = 24$ W m^{-2}; $\tau = \Delta H/Q \approx 24$ days.

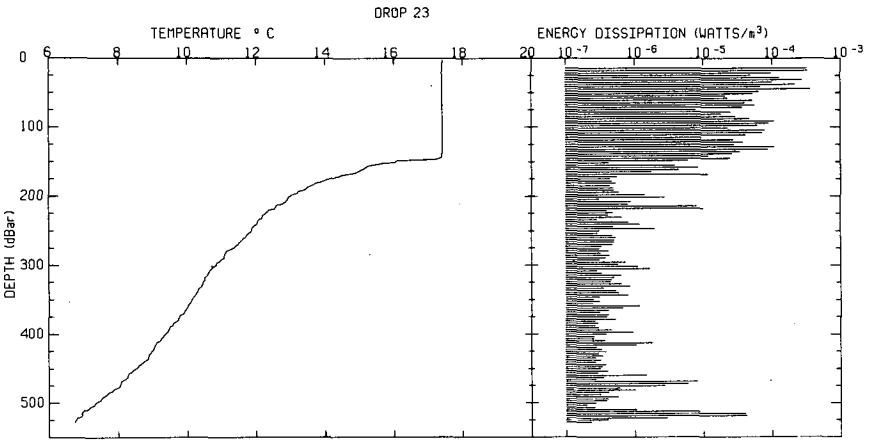

FIG. 12. A surface layer in a nearly complete state of mixing. From the surface to 135 m depth, temperature varies randomly between 17.380° and 17.397°. Turbulence does not cut off until 151 m, 1.6° "below" the mixing layer.

for mixing has vanished. The depth of the surface mixed layer is usually inferred from the location of a sharp temperature gradient in profiles made with XBTs, AXBTs or a CTD. A nearly isothermal layer is presumed to be turbulent and dissipating kinetic energy over its entire depth. Models of phytoplankton growth assume that the position of a plankton particle is, statistically, uniformly over the depth range of the mixed layer (Woods and Onken 1982). The plankton's average light exposure is then the depth-weighted mean light intensity in the mixed layer. However, if turbulence is limited to only a shallow surface layer, as in drop 10, then such a model greatly overestimates the photosynthesis of plankton in the isothermal layer below the surface mixing layer. Models of mixing-layer dynamics also will not properly simulate the distribution of turbulence found from drop 10 because these models consider only surface heating as the means to restratify a decaying surface mixed layer. However, a considerable heat flux out of the bottom of the mixed layer can be realized by turbulence in the top of the seasonal thermocline as is evident in drop 10. This heat flux is independent of the local air–sea interaction, depends on the internal wave climate, and can be a mechanism restratifying the mixed layer. The downward flux of heat, $H = \rho c_p \langle w'T' \rangle$, between 130 and 136 m can be estimated using the method of Osborn (1980). Setting the eddy diffusivity to $0.2\epsilon\rho^{-1}N^{-2}$ gives

$$H = \rho c_p (0.2\epsilon\rho^{-1}N^{-2})\partial\langle T\rangle/\partial z$$

$$= \frac{0.2\epsilon c_p}{\alpha g}\frac{R}{R-1} = 140 \text{ W m}^{-2},$$

where $R = \alpha T_z/\beta S_z$ and is estimated from Roden (1980b), $\alpha = \partial\sigma_t/\partial T$, $\beta = \partial\sigma_t/\partial S$ and c_p is the heat capacity. This turbulent flux is not small compared to typical daily mean surface fluxes. The near-inertial climate induced by storms will have to be considered in the modeling of the evolution of surface mixed layers, particularly at fronts where trapped waves are possible (Kunze and Sanford 1984).

d. Geographic variations

Models of circulation in general, and of fronts in particular, suffer to some extent from uncertainties of how to characterize turbulence in terms of the parameters of the larger flow field, such as the gradient Richardson number and the buoyancy frequency. The model of Garvine (1980), for example, has diffusion by turbulence restricted to a region of 0.25σ, where σ is the cross-frontal distance normalized by the baro-

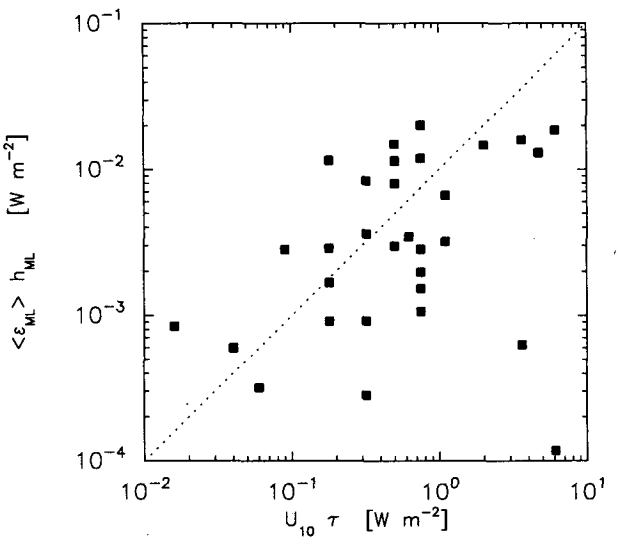

FIG. 13. The integral of dissipation over the mixing layer and the work done by the wind field at the bottom of the atmospheric boundary layer ($\tau \cdot U_{10}$). The dashed line corresponds to 1%.

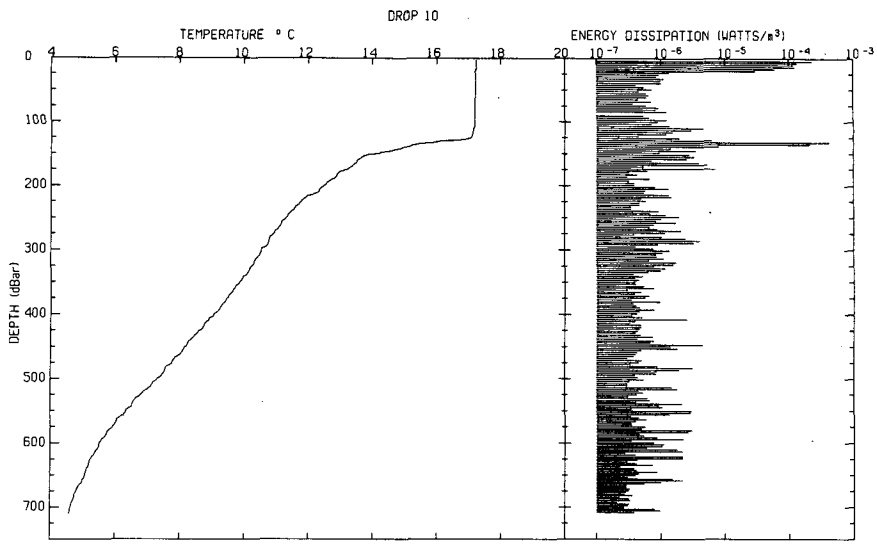

FIG. 14. A quasi-isothermal mixed layer that is actively turbulent in only the upper 20 m. The absence of dissipation shows that there is no Reynolds stress between 20 and 130 m depth. The strongest dissipative feature is between 130 and 136 m. This is the depth of a near-inertial wave with a Richardson number of 0.33 (Kunze and Sanford, personal communication 1984).

clinic Rossby radius. For the Pacific subtropical front this distance is only a few kilometers. Marmorino et al. (1985) observed patches of elevated temperature microstructure variance over a distance of several Rossby radii (24 km) on the cold side of a front in the Sargasso Sea. The sampling reported here is sparse, and so we can only attempt to see if turbulent dissipation varies over synoptic scale distances from the front. Dissipation as a function of distance from the subtropical front is summarized in Fig. 15. For each profile, the dissipation data have been averaged over three depth ranges. The first range spans the surface mixing layer and ranges from the surface to the depth at which either the dissipation is within a factor of 2 of the noise level, namely 4×10^{-7} W m^{-3}, or the temperature is 0.1°C less than at the surface. Thus the mixing layer depth can be less than the mixed layer depth. The second depth range spans from the bottom of the mixing layer to 300 m, which includes subducted mixed layers, if they are present. Hydrographic sections by Roden (1981) indicate that the subtropical front is only well defined in the upper 250 to 300 meters. The third depth range covers the remainder of the water column, where no trend is expected. Below the mixing layer there is no intensification of dissipation rates near the front compared to the far field. In the mixing layer and on the warm side of the front there is a suggestion of intensification during the second phase only. Because four of the five largest mean mixing layer dissipations were observed within a period of 24 hours, it is more likely that this intensification reflects variability of air–sea interactions rather than geographic variations.

Although no intensification of dissipation rates was observed near the Pacific subtropical front on synoptic scales, the data are not necessarily inconsistent with the observation of trapped near-inertial waves on the warm side of the front by Kunze and Sanford (1984). Between January 21 and 25, they observed large-amplitude waves in a 5 km wide band along the south side of the front. The dominant vertical wavelengths were 250 and 130 m, and the latter had a Richardson number of 0.25. Thus, the 35 km station spacing employed was far too sparse to resolve the feature reported by Kunze and Sanford. However, it is still possible that some of the profiles were made in the trapped waves. Shear magnitude will have a maximum every half wavelength in the vertical and so, layers of shear generated turbulence should be spaced 65 m. The profile from drop 29 (Fig. 16) shows five major dissipation maxima separated by approximately 65 meters. The regular spacial pattern in the dissipation is similar to observations from below the thermostat in a warm-core ring (Lueck and Osborn 1985) which were attributed to trapped near-inertial waves. Other profiles from drops at nearly the same surface isohaline as drop 29 show little regularity in the vertical spacing of the layers of dissipation.

e. Statistics

Although it is not possible to detect a frontal signature in the dissipation profiles around the front, the ensemble of the profiles may differ significantly from other regions. We will first examine the statistical distribution of dissipation for the three depth regions defined earlier and then compare the averages to data reported by others.

Monin and Yaglom (1975) report that dissipation rates in a fully developed turbulent boundary layer should follow a lognormal distribution. Osborn and Lueck (1985) were able to fit more than 80% of their 2673 dissipation estimates to a lognormal distribution when all samples were chosen from one 4.5 meter depth range in a surface mixing layer. Their data come from a 10 minute interval, and so surface forcing and other conditions were very uniform. Fitting dissipation data to a single lognormal distribution implies that the observations are drawn from one population, an unlikely condition in the thermocline where time varying shear induced by internal waves produces much of the turbulence. The frequency distribution of dissipation from the surface mixing layers appears to be lognormal (Fig. 17), even though the data were measured under wind speeds from 0 to 15 m s^{-1}. However, 65% of the data were measured when wind speeds were 7 m s^{-1} and higher. The bars in Fig. 17 represent the observed frequency density estimated over quarter decade bins. Observations below 3×10^{-7} W m^{-3} have been removed because they are partially contaminated by noise. The line fitted to the data is the probability density of the base 10 logarithm of dissipation computed from a linear fit to the cumulative probability distribution (Lueck and Osborn 1982). The line to the right is $\epsilon p(\log_{10}\epsilon)/\epsilon_s$ which represents the contribution towards the mean dissipation because $\epsilon p(\epsilon)d\epsilon = \epsilon p(\log_e\epsilon)d(\log_e\epsilon)$, where ϵ_s is the estimated mean given by $\int_0^\infty \epsilon p(\epsilon)d\epsilon$. Thus, the area under the right-hand curve is unity. This curve is displaced towards the right of the frequency distribution because large dissipation observations, although less frequent, can contribute significantly towards the average dissipation. The asterisk marks the largest observed value. If there is significant area under the second curve towards the right of the asterisk then the dataset has been inadequately sampled or is not represented by a lognormal distribution.

Even when a generous allowance is made for noise, the data from below the mixing layer (Figs. 17b and 17c) show a strong departure from a lognormal distribution by an excess of dissipation observations below 10^{-6} W m^{-3}. However, the mean dissipation rates predicted by the lognormal fit agree to within 10% with the observed ensemble populations means for both datasets from below the mixing layer. The close agreement between the observed means and the means computed from fits to the cumulative probability distributions does not support the contention of Baker and Gibson (1987) that the arithmetic means of turbulence statistics, such as dissipation rates, are subject to errors because of the skewness of turbulence parameters. The statistics of dissipation below the mixing layer must be more complex than a lognormal distribution. The local mechanism producing ocean turbulence will have to be positively identified before we can explain the statistics of thermocline dissipation rates.

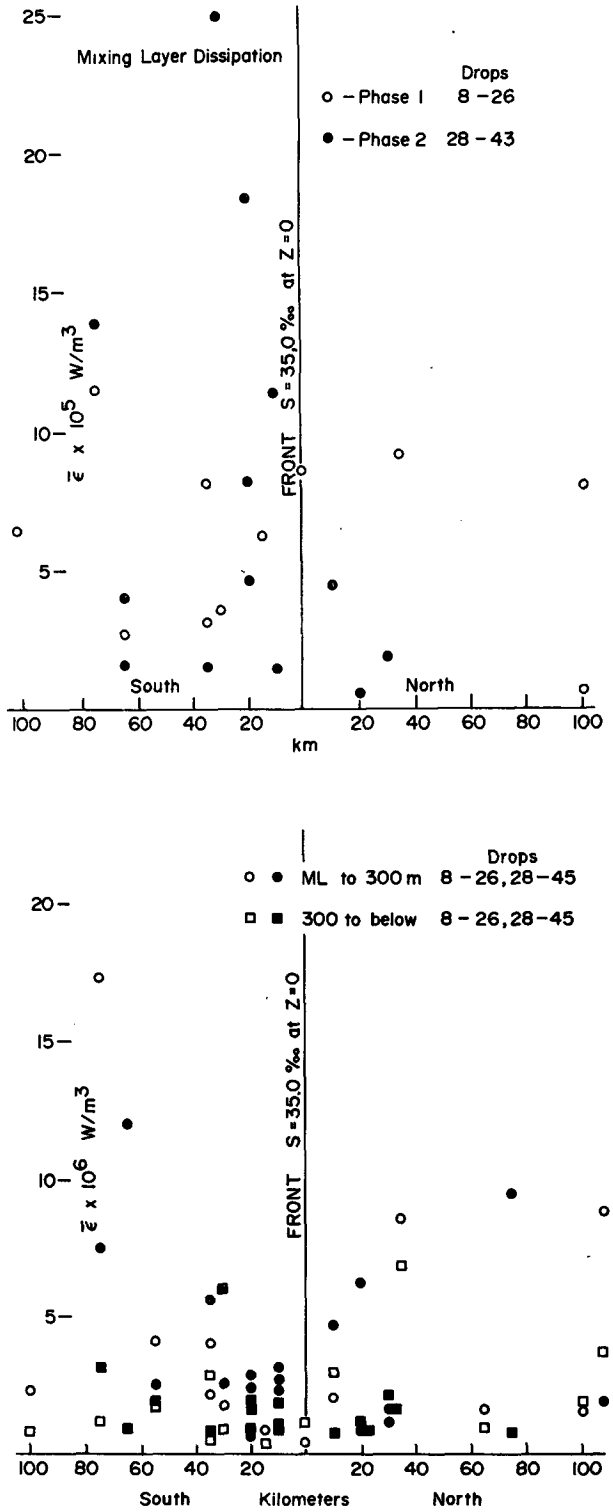

FIG. 15. Mean dissipation as a function of distance from the front as marked by the 35 surface isohaline. Direction is taken normal to the front, "north" referring to a station in water fresher than the front, and "south" as saltier than the front. Three depth ranges were chosen to separate effects due to local air-sea interaction from subsurface frontal effects: (a) mixing layer and (b) bottom of mixing layer to 300 m depth and below 300 m depth.

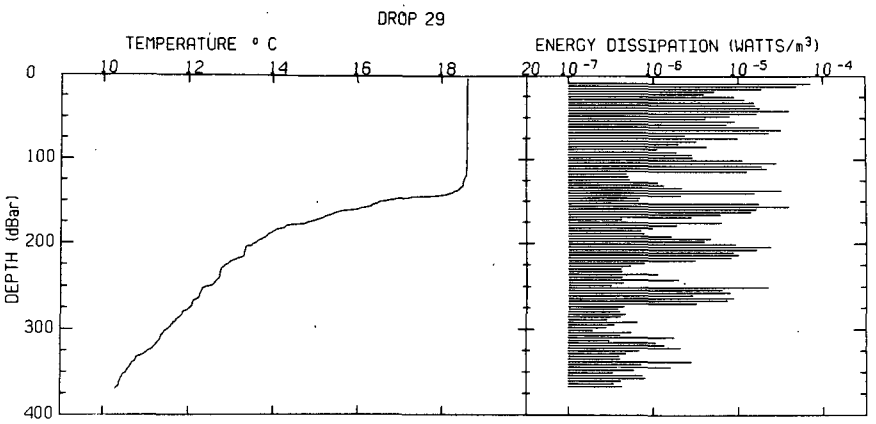

FIG. 16. Profile 29 on the warm edge of the front showing five layers of dissipation separated by 65 m in the vertical as predicted by the near-inertial wave observations of Kunze and Sanford (1985).

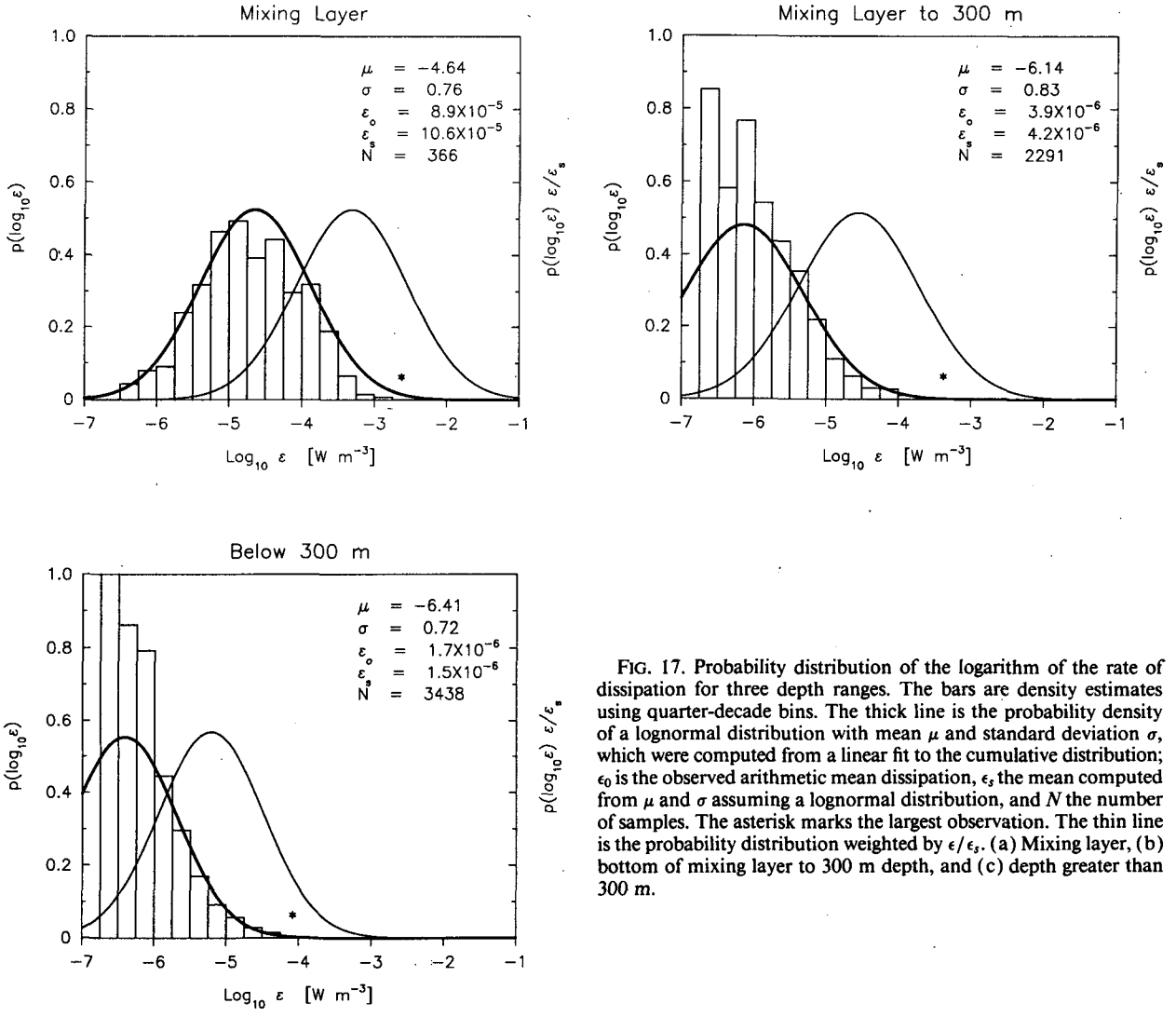

FIG. 17. Probability distribution of the logarithm of the rate of dissipation for three depth ranges. The bars are density estimates using quarter-decade bins. The thick line is the probability density of a lognormal distribution with mean μ and standard deviation σ, which were computed from a linear fit to the cumulative distribution; ϵ_0 is the observed arithmetic mean dissipation, ϵ_s the mean computed from μ and σ assuming a lognormal distribution, and N the number of samples. The asterisk marks the largest observation. The thin line is the probability distribution weighted by ϵ/ϵ_s. (a) Mixing layer, (b) bottom of mixing layer to 300 m depth, and (c) depth greater than 300 m.

TABLE 5. Mean dissipations and some standard deviations of lognormal fits for observations from various oceanic regions.

Region	Depth range (m)	$10^7\langle\epsilon\rangle$ (W m^{-3})	STD log(ϵ) (base 10)	Source
Pacific subtropical front	ML	890	0.76	
	ML–300	39	0.83	
	300–1000	17	0.72	
Pacific equator	40–120	1000	1.0	Crawford (1982)
Azores	150–500	56	0.75	Osborn (1978)
Sargasso Sea	50–1100	1		Gargett and Osborn (1981)
Seasonal thermocline	32–36	510	0.30	Osborn and Lueck (1985b)
Surface mixing layer	28–32	890	0.61	Osborn and Lueck (1985a)
Continental slope	100–200	18		Lueck et al. (1983)
	200–500	5.3		
	500–1000	2.8		
Warm-core ring	Thermocline	40		Lueck and Osborn (1986)
	Edge	120		
	Thermostat	2		

The means and standard deviations for the frontal observations are compared against others in Table 5. Average dissipation at the front is greater than dynamically inactive areas such as off Vancouver Island and the Sargasso Sea, but is less compared to very active regimes such as the Equatorial Undercurrent or a warm-core ring.

4. Conclusions

Water is advected across the North Pacific subtropical front by the subduction of surface mixed layers from the north side of the front underneath surface mixed layers on the south side. The signature of this differential motion is provided by the thick quasi-isothermal structure found in surface mixed layers. Cross-frontal penetration of thermocline water cannot be identified in hydrographic data because the θ–S relationship does not vary across the front. This interleaving of the surface mixed layers converts relatively large cross-frontal horizontal property gradients into even larger vertical gradients. When surface winds are moderate, less than 10 m s^{-1}, turbulence in the transition layer separating surface from subsurface mixed layers is too small to effectively mix these layers. However, strong vertical mixing was observed when wind speeds reached 15 m s^{-1}. The time scale for mixing is then estimated to be only 24 days and even less for winds too severe to permit measurements. It is thus possible that thermal frontogenesis generated by horizontal convergence is diffused by vertical mixing generated by air–sea interaction.

The deepest surface mixing layer reached to 145 m. When the entire surface isothermal layer was turbulent then, turbulence also extended several meters further into the seasonal thermocline. Many surface mixed layers were not measurably turbulent over their entire depth. For these cases, turbulence in the mixed layers was restricted to a shallow layer in contact with the surface and turbulence was also observed just below the base of the mixed layer. Because there was no wind induced shear stress in the lower portions of the mixed layer, turbulence near the base of the mixed layer was not related to local air–sea interaction. In at least one profile, mixing at the top of the thermocline was associated with a near-inertial wave.

Depth averaged dissipation rates from individual profiles do not show a dependence on distance from the front. The station spacing of 37 km employed for this study was too coarse to resolve any mixing that may have been produced by near-inertial waves that are trapped on the warm side of the front by large scale vorticity. The ensemble average of thermocline dissipation rates in the subtropical front is larger than that found in regions of low energetics such as the Sargasso Sea, but is smaller than found in highly energetic regions such as the Equatorial Undercurrent or a warm-core ring.

The dissipation rates from turbulent surface mixing layers follows a lognormal distribution. Observations from the thermocline deviate from a lognormal distribution for small dissipation values. However, means predicted by a lognormal fit agree to within 10% with arithmetic averages. The vertical integral of dissipation rates in the surface mixing layers is approximately 1% of the work done by the surface wind field, in agreement with other measurements.

Acknowledgments. I should like to acknowledge help from the following: 1) Gunnar Roden, Chief Scientist on the R/V *Thomas Washington,* for co-operation and useful discussions during the cruise and for use of his CTD data. 2) Capt. Phinney and his crew for the excellent maneuvering of their ship during the recovery

and landing of *Camel II*. 3) B. Anderson and R. Lakowski, formerly with the University of British Columbia, and the PCODF group of Scripps for technical assistance during the cruise. 4) S. Millaire and B. Anderson for helping build *Camel II* and R. Lakowski for programming and data analysis. This work was supported by the Office of Naval Research under Contract N00014-76-C-0446 and others.

REFERENCES

Baker, M. A., and C. H. Gibson, 1987: Sampling turbulence in a stratified ocean: Statistical consequences of strong intermittency. *J. Phys. Oceanogr.*, **17**, 1817–1836.

Flament, P., L. Armi and L. Washburn, 1985: The evolving structure of an upwelling filament. *J. Geophys. Res.*, **90**, 11 765–11 778.

Crawford, W. R., 1982: Pacific equatorial turbulence. *J. Phys. Oceanogr.*, **12**, 1137–1149.

Gargett, A. E., and T. R. Osborn, 1981: Small-scale shear measurements during the Fine and Microstructure Experiment (FAME). *J. Geophys. Res.*, **86**, 1929–1944.

Garvine, R. W., 1980: The circulation dynamics and the thermodynamics of upper ocean density fronts. *J. Phys. Oceanogr.*, **10**, 2058–2081.

Gregg, M. C., E. A. D'Asaro, T. J. Shay and N. Larson, 1986: Observation of persistent mixing and near-inertial internal waves. *J. Phys. Oceanogr.*, **16**, 856–885.

Hayes, S. P., G. Roden and C. A. Paulson, 1981: Shipboard meteorological observations. FRONTS-80: Preliminary Results from an Investigation of the Wintertime North Pacific Subtropical Front. C. A. Paulson and P. P. Niiler, Eds., School of Oceanography Report 81-2, Oregon State University, Corvallis, OR, 97331.

Kunze, E., and T. B. Sanford, 1984: Observation of near-inertial waves in a front. *J. Phys. Oceanogr.*, **14**, 566–581.

Lueck, R. G., and T. R. Osborn, 1982: Dissipation measurements from the FRONTS-80 expedition. U.B.C., Department of Oceanography Manuscript Report No. 38.

——, and ——, 1985: Dissipation of kinetic energy in a warm-core ring. *J. Geophys. Res.*, **91**, 803–818.

——, W. C. Crawford and T. R. Osborn, 1983: Turbulent dissipation over the continental slope off Vancouver Island. *J. Phys. Oceanogr.*, **13**, 1809–1818.

Marmorino, G. O., L. J. Rosenblum, J. P. Dugan and C. Y. Shen, 1985: Temperature fine-structure patches near an upper ocean density front. *J. Geophys. Res.*, **90**, 11 799–11 810.

Monin, A. S., and A. M. Yaglom, 1975: *Statistical Fluid Mechanics, Vol. 2*, MIT Press, 873 pp.

Moum, J. N., and D. R. Caldwell, 1985: Local influences on shear-flow turbulence in the equatorial ocean. *Science*, **230**, 315–316.

——, and R. G. Lueck, 1985: Causes and implications of noise in oceanic dissipation measurements. *Deep-Sea Res.*, **32**, 379–390.

Oakey, N. S., 1985: Statistics of mixing parameters in the upper ocean during JASIN phase 2. *J. Phys. Oceanogr.*, **15**, 1662–1675.

——, and J. A. Elliott, 1980: Dissipation in the mixed layer near Emerald basin. *Marine Turbulence*, J. C. J. Nihoul, Ed., Elsevier Scientific.

——, and ——, 1982: Dissipation within the surface mixed layer. *J. Geophys. Res.*, **12**, 171–185.

Osborn, T. R., 1978: Measurements of energy dissipation adjacent to an island. *J. Geophys. Res.*, **83**, 2939–2957.

——, 1980: Estimates of the local rate of diffusion from dissipation measurements. *J. Phys. Oceanogr.*, **10**, 83–89.

——, and W. R. Crawford, 1980: An airfoil probe for measuring turbulent velocity fluctuations in water. *Air–Sea Interactions: Instruments and Methods*, F. Dobson, L. Hasse, and R. Davis, Eds., Plenum Press, 801 pp.

——, and R. G. Lueck, 1985a: Turbulence measurements with a submarine. *J. Phys. Oceanogr.*, **15**, 1502–1520.

——, and ——, 1985b: Turbulence measurements from a towed body. *J. Atmos. Oceanic Technol.*, **2**, 517–527.

Roden, G. I., 1975: On the North Pacific temperature, salinity, sound velocity and density fronts and their relationship to the wind and energy flux fields. *J. Phys. Oceanogr.*, **5**, 557–571.

——, 1980a: On the subtropical frontal zone north of Hawaii during winter. *J. Phys. Oceanogr.*, **10**, 342–362.

——, 1980b: FRONTS Expedition, CTD Data Report, Depart. of Ocean., University of Washington, Contribution No. 1167.

——, 1981: Mesoscale thermohaline, sound velocity and baroclinic flow structure of the Pacific Subtropical front during winter of 1980. *J. Phys. Oceanogr.*, **11**, 658–675.

Rohr, J. J., K. N. Helland, E. C. Itsweire and C. W. van Atta, 1987: Turbulence in a stably stratified shear flow: A progress report. *Turbulent Shear Flows*, Springer-Verlag.

Shay, T. J., and M. C. Gregg, 1986: Convectively driven turbulent mixing in the upper ocean. *J. Phys. Oceanogr.*, **16**, 1777–1798.

Stillinger, D. C., K. N. Helland and C. W. van Atta, 1983: Experiments on the transition of homogeneous turbulence to internal waves in a stratified fluid. *J. Fluid Mech.*, **131**, 91–122.

van Woert, M., 1982: The subtropical front: Satellite observations during FRONTS 80. *J. Geophys. Res.*, **87**, 9523–9536.

Woods, J. D., and R. Onken, 1982: Diurnal variation and primary production in the ocean—preliminary results of a Lagrangian ensemble model. *J. Plankton Res.*, **4**, 735–736.